A Study into the Method of Precise Orbit Determination of a HEO Orbiter by GPS and Accelerometer

Toshinori Ikenaga*, Yoshi Hashida** and Martin Unwin**
* JAXA (Japan Aerospace Exploration Agency), ** SSTL(Surrey Satellite Technology Ltd)

1. Introduction

In the present day, orbit determination by Global Positioning System (GPS) is not unusual. Especially for low-cost small satellites, position determination by an on-board GPS receiver provides a cheap, reliable and precise method. However, the original purpose of GPS is for ground users, so the transmissions from all of the GPS satellites are directed toward the Earth's surface. Hence there are some restrictions for users above the GPS constellation to detect those signals. On the other hand, a desire for precise orbit determination for users in orbits higher than GPS constellation exists. For example, the next Japanese Very Long Baseline Interferometry (VLBI) mission "ASTRO-G" is trying to determine its orbit in an accuracy of a few centimetres at apogee. The use of GPS is essential for such ultra accurate orbit determination. This study aims to construct a method for precise orbit determination for such high orbit users, especially in High Elliptical Orbits (HEOs). There are several approaches for this objective. In this study, a hybrid method with GPS and an accelerometer is chosen. Basically, while the position cannot be determined by an on-board GPS receiver or other Range and Range Rate (RARR) method, all we can do to estimate the user satellite's position is to propagate the orbit along with the force model, which is not perfectly correct. However if it has an accelerometer (ACC), the coefficients of the air drag and the solar radiation pressure applied to the user satellite can be updated and then the propagation along with the "updated" force model can improve the fitting accuracy of the user satellite's orbit. In this study, it is assumed to use an accelerometer available in the present market. The effects by a bias error of an accelerometer will also be discussed in this paper.

Table 1-1-1: Osculating Keplerian Orbital Elements

Epoch	00:00:00.0, 16th, May, 2006
Semi-major Axis	19378.0 km
Eccentricity	0.62
Inclination	31.0
RAAN	0.0
Argument of Perigee	0.0
Mean Anomaly	0.0

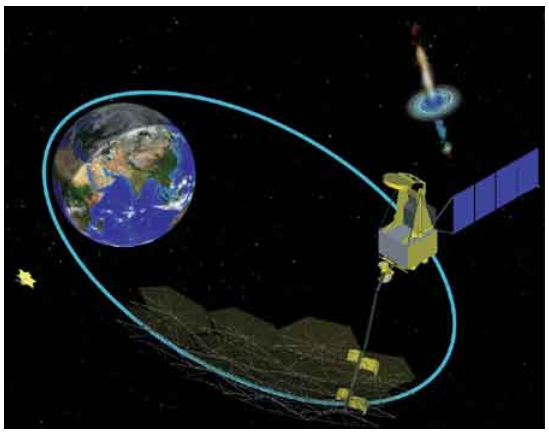

Figure 1-1-1: Image of ASTRO-G

In this study, the next Japanese VLBI mission called "ASTRO-G" is used as a test mission. VLBI is a method of astronomical observation in the field of radio astronomy. The first VLBI mission was conducted

by Japanese satellite called "HALCA" which was the first VLBI satellite and finished its mission in 2005 after 8 years operation.

ASTRO-G is also planned by ISAS / JAXA, and it is scheduled to be launched in 2011. The orbit type of this mission is HEO, and the required orbit determination accuracy is a few centimetres at apogee. Figure 1-1-1 shows the image of this mission.

In Table 1-1-1 the osculating Keplerian orbital elements of ASTRO-G's orbit are summarised. As you can see in this table, the perigee altitude is 1,000 km while the apogee altitude is 25,000 km which is higher than the altitude of GPS orbits. The epoch time shown in Table 1-2-1 is the time set for this study.

Figure 1-1-2 shows us the geometric relationship between the Earth, GPS satellite and ASTRO-G.

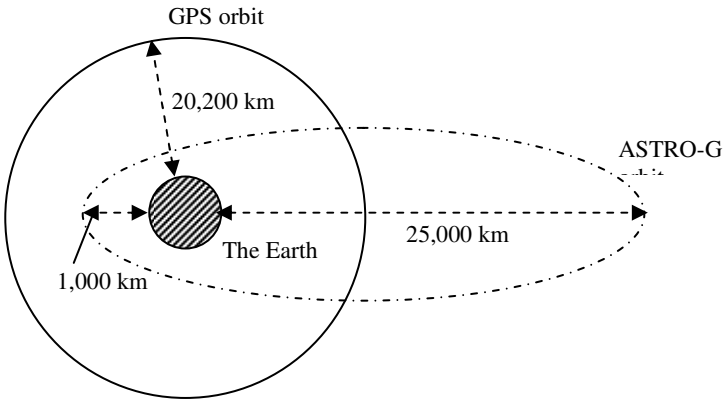

Figure 1-1-2: Conceptual Diagram of GPS & ASTRO-G orbits

In this study, it is intended to determine the orbit by using both of the GPS measurement data collected in the "lower" part of the orbit and the on-board ACC output data. The ACC allows to estimate more suitable force model, which will improve the orbit determination accuracy.

2. Perturbation Forces

In real situation, several perturbation forces are also applied to a satellite. When those forces are taken into account, the force vector $\vec{a}$ is described as;

$$\vec{a} = -\frac{\mu_E}{r^3}\vec{r} + \vec{a}_{nonspherical} + \vec{a}_{3-body(Sun)} + \vec{a}_{3-body(Moon)} + \vec{a}_{airdrag} + \vec{a}_{SR} \qquad (2\text{-}1)$$

where, $\vec{a}_{nonspherical}$ is the perturbation force cause by the non-spherical terms of the geo-potential model, $\vec{a}_{3-body(Sun)}$ and $\vec{a}_{3-body(Moon)}$ are the forces by the third bodies, specifically the Sun and the Moon. $\vec{a}_{airdrag}$ is the force caused by the Earth's atmosphere and $\vec{a}_{SR}$ is the solar radiation pressure.

When we design the estimator utilizing ACC we have to consider the two disturbing forces i.e. the Air drag and the Solar radiation pressure. In the following sections those forces are introduced.

2-1 Air Drag

The disturbing force by the atmospheric drag has a strong influence against the motion of the LEO satellites. The next equation describes this perturbation force;

$$\vec{a}_{airdrag} = -\frac{1}{2}\frac{C_D A}{m}\rho v^2{}_{rel}\frac{\vec{v}_{rel}}{|\vec{v}_{rel}|} \tag{2-1-1}$$

where C_D is the coefficient of drag which describe the susceptibility of the satellite to the air drag force. C_D is approximately 2.2 in the upper atmosphere of the Earth when a flat plate model is applied. A is the cross-sectional area exposed to the atmosphere, and m is the mass of the satellite. ρ is the atmospheric density which differs along with the altitude. $\vec{v}_{rel}$ is the velocity vector of the satellite relative to the atmosphere. This velocity vector is also described in the Earth Centred Inertial (ECI) coordinate system in this research.

In this study, the following parameters are used;

$$A = 50.0\left(m^2\right) \qquad m = 830.0(kg) \tag{2-1-2}$$

These values are derived from HALCA's specification.

Practically speaking, the atmospheric density ρ changes depending on the complicated interaction among some basic factors. However, in this research, simple values are used which changes with the altitude for simplicity. Figure 2-1-1 summarises the values of the mean atmospheric density [2]. And the derivative of $\vec{a}_{airdrag}$ by $\vec{r}_{sat}$ is zero.

In this research the atmospheric density is interpolated linearly by using the values of Figure 2-1-1. The altitude above 1500km, it is defined that the density lineally reduces and reaches zero at the altitude 1750km.

For the simulation of this study the following description is used for simplicity.

$$\vec{a}_{airdrag} = -K_{drag}|\vec{v}_{sat}|\vec{v}_{sat} \tag{2-1-3}$$

The K_{drag} appearing in the equation (2-1-3) is one of the state parameters estimated by the orbit estimator.

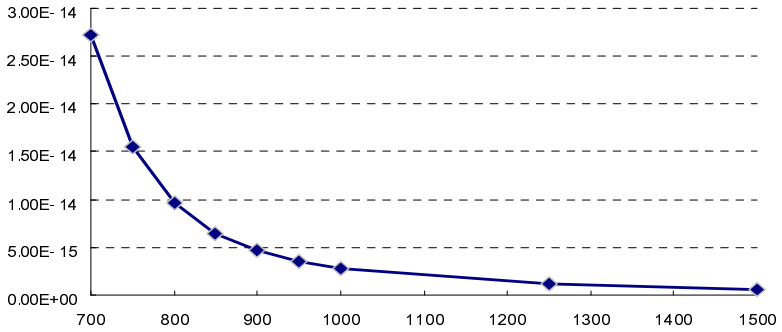

Figure 2-1-1: Mean Atmospheric Density

2-2 Solar Radiation Pressure

The radiation from the Sun also affects on the satellite motion as a perturbing force. The solar-radiation pressure is given by;

$$\vec{a}_{SR} = -\frac{p_{SR}C_R A_{Sun}}{m}\frac{\vec{r}_{sat-Sun}}{|\vec{r}_{sat-Sun}|} \tag{2-2-1}$$

where p_{SR} is the solar pressure which equals to $4.51\times10^{-6}\ N/m^2$. C_R is the reflectivity whose value is between 0.0 to 2.0. In this research the C_R is set to 1.3. A_{Sun} is the satellite's exposed area to the Sun and m is satellite's mass. These A_{Sun} and m are same as the values shown in (2-1-2). $\vec{r}_{sat-Sun}$ is the point vector from the satellite to the Sun. The derivative of $\vec{a}_{SR}$ is zero.

This perturbation force is also written in the following equation (2-4-2). The coefficient K_{SRP} is estimated by the orbit estimator in this study.

$$\vec{a}_{SR} = -K_{SRP}\frac{\vec{r}_{sat-Sun}}{|\vec{r}_{sat-Sun}|} \tag{2-4-2}$$

3. Visibility Analysis

3-1 Geometry

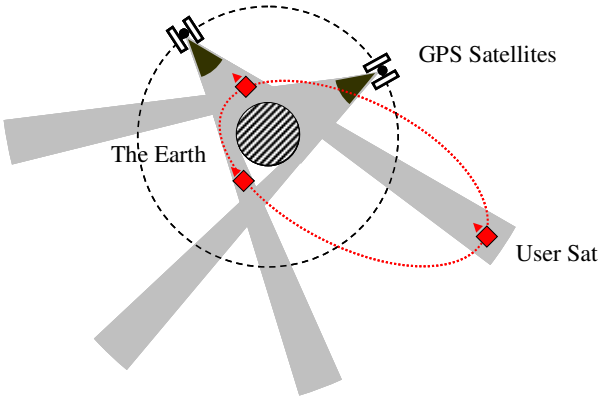

Figure 3-1: Geometrical Allocation of GPS satellites and the user satellite

To evaluate the feasibility of the orbit estimator designed in this study, the visibility analysis of GPS satellites should be investigated. Figure 3-1 shows the geometrical allocations of the GPS satellites and the user satellite. As can be seen, the user above the GPS orbits can only detect the signal from the GPS satellite which is beyond the Earth because all of the GPS signal transmission is directed toward the Earth, beside the beam width of the transmission antenna is not so wide.

3-2 GPS Antenna Configuration

To analyse the visibility of the GPS satellites in detail, the antenna patterns of the GPS transmission antenna and the GPS receiver's antenna are defined. As far as I know, the antenna configuration of the on-board GPS satellite antenna is not published. However some results of the investigation by GPS users are published. Basically, the antenna pattern for the GPS signal transmission should be designed to illuminate the Earth's surface from the altitude 20,200km. Hence the half angle should be about 13.88 degrees. Figure 3-2-1 shows the antenna geometry.

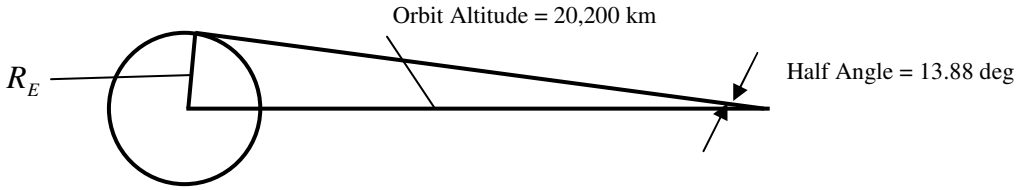

Figure 3-2-1: The Geometry of the GPS transmission antenna

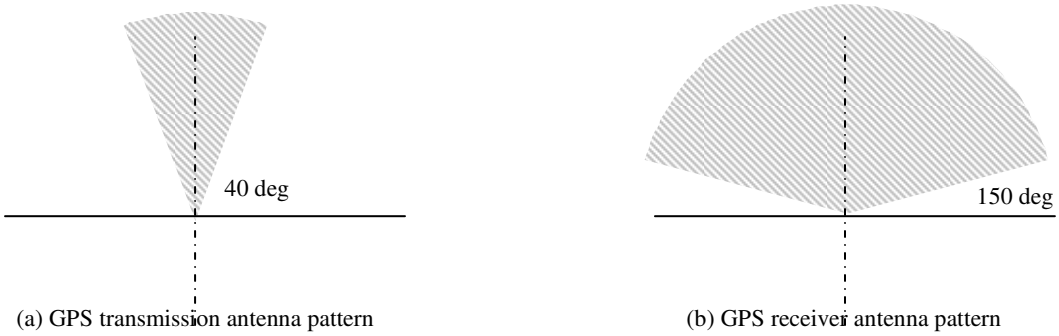

(a) GPS transmission antenna pattern (b) GPS receiver antenna pattern

Figure 3-2-2: Diagram of Antenna Patterns

On the other hand, the beamwidth of GPS receiver's antenna is set to 150 degrees. Figures 3-2-2 shows the diagram of those antenna patterns.

To figure out the visible number of GPS satellites, the shape of the satellite and the coordinate system was determined as shown in Figure 3-2-3.

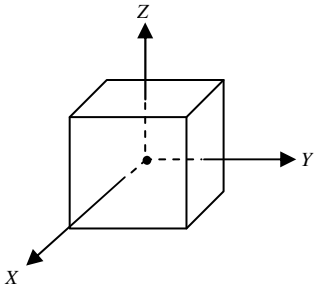

Antenna Loading Facets

Considered 6 antennas are loaded on all facets i.e.
+ X & - X facets
+ Y & - Y facets
+ Z & - Z facets

Figure 3-2-3: Definition of Coordinate System of the satellite

As summarised in Figure 3-2-3, it is considered 6 GPS antennas are loaded on 6 panels of a cubed shape satellite. The satellite's body frame is fixed in the inertial space and the user satellite's shape is simply assumed a cube. Figure 3-2-4 shows the result of the visibility analysis.

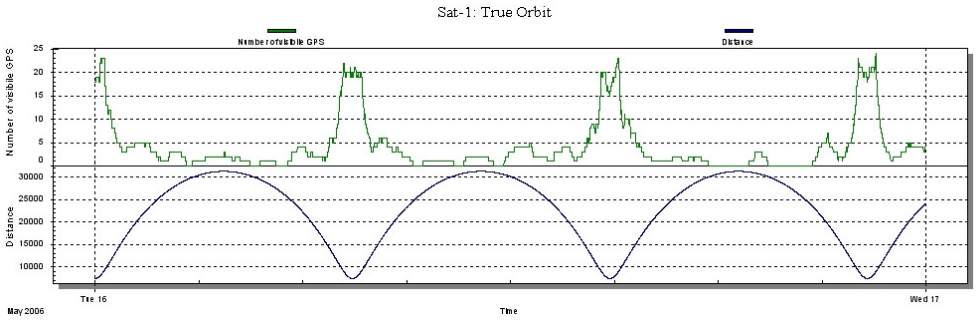

Figure 3-2-4: Result of Visibility Analysis

4. Orbit Estimator

4-1 Kalman Filtering

The orbit estimator designed in this study uses Kalman Filtering method. Kalman Filtering is a technique for computing the best estimate of the state parameters from imperfect observation values and uncertain dynamic model. Figure 4-1-1 shows the flow chart of this method.

In this study, the state parameters are the range and velocity vectors of the user satellite, and two coefficients of the air drag and the solar radiation pressure. The subscripts "drag" and "SRP" appearing in Figure 4-1-1 describe the air drag and the solar radiation pressure respectively. On the other hand, the observation values are the range, velocity and acceleration vectors. Note that the range and velocity vectors are described in ECI coordinate system while the acceleration vector's coordinate system is in the satellite's body frame.

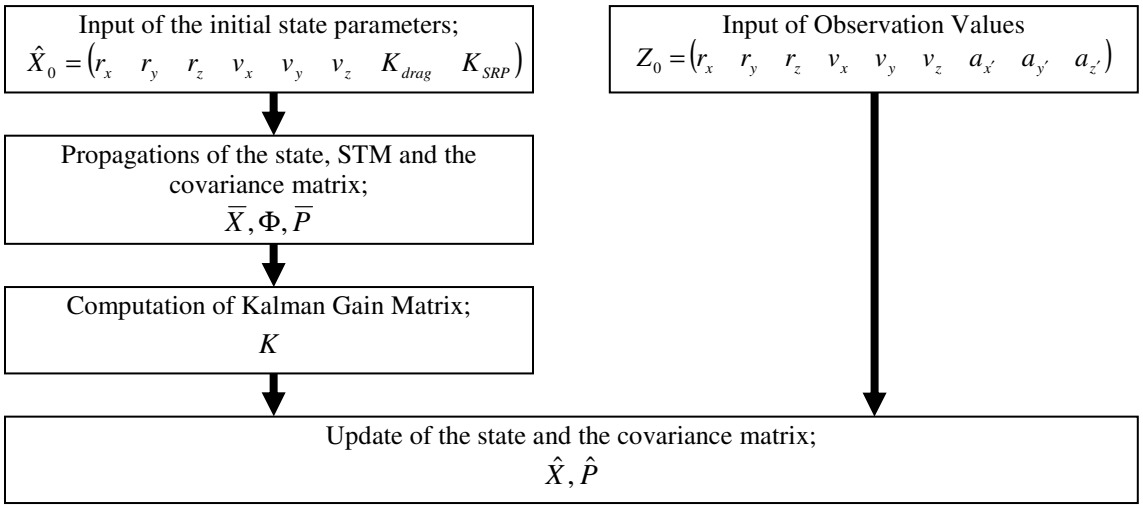

Figure 4-1-1: Flow Chart of Kalman Filtering

4-2 Observation Matrix

The observation matrix H is the matrix which describes the relationship between the state parameter X and the observation value Z. This matrix is defined by the following equation;

$$H = \frac{\partial Z}{\partial X} \tag{4-2-1}$$

In this study this matrix is;

$$H = \begin{bmatrix} \frac{\partial Z}{\partial \vec{r}} & \frac{\partial Z}{\partial \vec{v}} & \frac{\partial Z}{\partial K_{drag}} & \frac{\partial Z}{\partial K_{SRP}} \end{bmatrix} = \begin{bmatrix} \frac{\partial \vec{r}}{\partial \vec{r}} & \frac{\partial \vec{r}}{\partial \vec{v}} & \frac{\partial \vec{r}}{\partial K_{drag}} & \frac{\partial \vec{r}}{\partial K_{SRP}} \\ \frac{\partial \vec{v}}{\partial \vec{r}} & \frac{\partial \vec{v}}{\partial \vec{v}} & \frac{\partial \vec{v}}{\partial K_{drag}} & \frac{\partial \vec{v}}{\partial K_{SRP}} \\ \frac{\partial \vec{a}'}{\partial \vec{r}} & \frac{\partial \vec{a}'}{\partial \vec{v}} & \frac{\partial \vec{a}'}{\partial K_{drag}} & \frac{\partial \vec{a}'}{\partial K_{SRP}} \end{bmatrix} \tag{4-2-2}$$

Note that the acceleration $\vec{a}'$ appearing in the equation (4-2-2) is the force by the air drag and the solar radiation pressure only because the on-board ACC can only detect the non-conservative forces which are not proportional to the satellite's mass. Hence this force is described by;

$$\vec{a}' = -K_{drag} |\vec{v}_{sat}| \vec{v}_{sat} - K_{SRP} \frac{\vec{r}_{sat-sun}}{|\vec{r}_{sat-sun}|} \tag{4-2-3}$$

To distinguish this force from the acceleration of the force model the notation "dash" is used. By substituting the equation (4-2-3) into (4-2-2), then the following matrix is obtained;

$$H = \begin{bmatrix} I_{3x3} & O_{3x3} & O_{3x1} & O_{3x1} \\ O_{3x3} & I_{3x3} & O_{3x1} & O_{3x1} \\ O_{3x3} & M_v & M_{drag} & M_{SRP} \end{bmatrix} \tag{4-2-4}$$

where;

$$M_v = -K_{drag} \begin{bmatrix} \frac{v_x^2}{|\vec{v}_{sat}|} + |\vec{v}_{sat}| & \frac{v_x v_y}{|\vec{v}_{sat}|} & \frac{v_x v_z}{|\vec{v}_{sat}|} \\ \frac{v_y v_x}{|\vec{v}_{sat}|} & \frac{v_y^2}{|\vec{v}_{sat}|} + |\vec{v}_{sat}| & \frac{v_y v_z}{|\vec{v}_{sat}|} \\ \frac{v_z v_x}{|\vec{v}_{sat}|} & \frac{v_z v_y}{|\vec{v}_{sat}|} & \frac{v_z^2}{|\vec{v}_{sat}|} + |\vec{v}_{sat}| \end{bmatrix} \tag{4-2-5}$$

$$M_{drag} = -|\vec{v}_{sat}| \begin{bmatrix} v_x \\ v_y \\ v_z \end{bmatrix} \qquad M_{SRP} = -\frac{1}{|\vec{r}_{sat}|} \begin{bmatrix} r_x \\ r_y \\ r_z \end{bmatrix} \tag{4-2-6}$$

4-3 State Transition Matrix

When we define the state transition matrix for 6 orbital parameters as Φ_{car}, then this matrix can be obtained by solving the following equation;

$$\dot{\Phi}_{car} = F\Phi_{car} \tag{4-3-1}$$

where;

$$F = \frac{\partial(\dot{\vec{r}}, \dot{\vec{v}})}{\partial(\vec{r}, \vec{v})} = \begin{bmatrix} \frac{\partial \dot{\vec{r}}}{\partial \vec{r}} & \frac{\partial \dot{\vec{r}}}{\partial \vec{v}} \\ \frac{\partial \dot{\vec{v}}}{\partial \vec{r}} & \frac{\partial \dot{\vec{v}}}{\partial \vec{v}} \end{bmatrix} = \begin{bmatrix} O_{3x3} & I_{3x3} \\ \frac{\partial \vec{a}}{\partial \vec{r}} & O_{3x3} \end{bmatrix} \tag{4-3-2}$$

The vector $\vec{a}$ appearing in the equation (4-3-2) is the force vector shown in the section 3. The matrices O_{3x3} and I_{3x3} are 3x3 zero matrix and the 3x3 identity matrix respectively. As can be seen in this equation we need to calculate the derivative of the force vector by the position vector of the user satellite to get the state transition matrix.

When we describe the state transition matrix with four 3x3 matrices, the equation (4-3-1) is modified into the following equation;

$$\begin{bmatrix} \dot{\Phi}_{11} & \dot{\Phi}_{12} \\ \dot{\Phi}_{21} & \dot{\Phi}_{22} \end{bmatrix} = \begin{bmatrix} O_{3x3} & I_{3x3} \\ D & O_{3x3} \end{bmatrix} \cdot \begin{bmatrix} \Phi_{11} & \Phi_{12} \\ \Phi_{21} & \Phi_{22} \end{bmatrix} \tag{4-3-3}$$

where $D = (\partial \vec{a} / \partial \vec{r}) I_{3x3}$. From the equation (4-3-3) we can obtain the state transition matrix Φ_{car}. On the other hand, the state transition matrix Φ_{ds} for the two coefficients of the air drag and the solar radiation pressure is simply described as following;

$$\Phi_{ds} = \begin{bmatrix} 1 & 0 \\ 0 & 1 \end{bmatrix} \tag{4-3-4}$$

because they are simply assumed constant. Consequently, the state transition matrix Φ in this study is written as;

$$\Phi = \begin{bmatrix} \Phi_{car} & O_{6x2} \\ O_{2x6} & \Phi_{ds} \end{bmatrix} \tag{4-3-5}$$

4-4 Process Noise Matrix

The matrix Q is a process noise matrix which describes uncertainty of the dynamic model in the orbit estimator. According to [7], the formula of this matrix is provided as;

$$Q_k = \int_{t_k}^{t_{k+1}} \int_{t_k}^{t_{k+1}} \Phi(t_{k+1}, \xi) E\left[\vec{u}(\xi)\vec{u}^T(\eta)\right] \Phi^T(t_{k+1}, \eta) d\xi d\eta \tag{4-4-1}$$

where the vector $\vec{u}$ is a noise vector whose elements are white Gaussian noise. Here, we assume that the process noise emerges only in the vector $\vec{w}$ because the uncertainty of the model is in the force i.e. $\vec{a}$. Hence the simplified orbit dynamics can be written;

$$\dot{\vec{r}} = \vec{v}, \quad \dot{\vec{v}} = \vec{w} \tag{4-4-2}$$

then we obtain;

$$E\left[u(\xi)u^T(\eta)\right] = \begin{bmatrix} O_{3x3} & O_{3x3} \\ O_{3x3} & S_p \delta(\xi - \eta) I_{3x3} \end{bmatrix} \tag{4-4-3}$$

where S_p is the spectral amplitude associated with the white noise driving function, and δ is Dirac delta function. $\vec{u}$ is specifically written as;

$$\vec{u}(\xi) = \begin{pmatrix} 0 & 0 & 0 & w_x(\xi) & w_y(\xi) & w_z(\xi) \end{pmatrix} \tag{4-4-4}$$

δ becomes "1" only when $\xi = \eta$. Therefore, the following equation is obtained from the equation (4-4-1);

$$Q_k = \begin{bmatrix} \frac{1}{3}S_p\Delta t^3 I_{3x3} & 0 & 0 & \frac{1}{2}S_p\Delta t^2 I_{3x3} & 0 & 0 \\ 0 & \frac{1}{3}S_p\Delta t^3 I_{3x3} & 0 & 0 & \frac{1}{2}S_p\Delta t^2 I_{3x3} & 0 \\ 0 & 0 & \frac{1}{3}S_p\Delta t^3 I_{3x3} & 0 & 0 & \frac{1}{2}S_p\Delta t^2 I_{3x3} \\ \frac{1}{2}S_p\Delta t^2 I_{3x3} & 0 & 0 & S_p\Delta t I_{3x3} & 0 & 0 \\ 0 & \frac{1}{2}S_p\Delta t^2 I_{3x3} & 0 & 0 & S_p\Delta t I_{3x3} & 0 \\ 0 & 0 & \frac{1}{2}S_p\Delta t^2 I_{3x3} & 0 & 0 & S_p\Delta t I_{3x3} \end{bmatrix} \tag{4-4-5}$$

4-5 Observation Noise Matrix

The matrix R is an observation noise matrix which corresponds to the sensor's noise used in the observation. This matrix is described as following;

$$R = \begin{bmatrix} M_{rng} & O_{3x3} & O_{3x3} \\ O_{3x3} & M_{vel} & O_{3x3} \\ O_{3x3} & O_{3x3} & M_{acc} \end{bmatrix} \tag{4-5-1}$$

where;

$$M_{rng} = \begin{bmatrix} r_{along-err} & 0 & 0 \\ 0 & r_{cross-err} & 0 \\ 0 & 0 & r_{radial-err} \end{bmatrix} \quad (4\text{-}5\text{-}2)$$

$$M_{vel} = \begin{bmatrix} v_{along-err} & 0 & 0 \\ 0 & v_{cross-err} & 0 \\ 0 & 0 & v_{radial-err} \end{bmatrix} \quad (4\text{-}5\text{-}3)$$

$$M_{acc} = \begin{bmatrix} a'_{along-err} & 0 & 0 \\ 0 & a'_{cross-err} & 0 \\ 0 & 0 & a'_{radial-err} \end{bmatrix} \quad (4\text{-}5\text{-}4)$$

5. Simulation

5-1 Simulation Configuration

To figure out the contribution of an on-board ACC some simulations are carried out. Figure 5-1-1 shows the diagram of the simulation configuration.

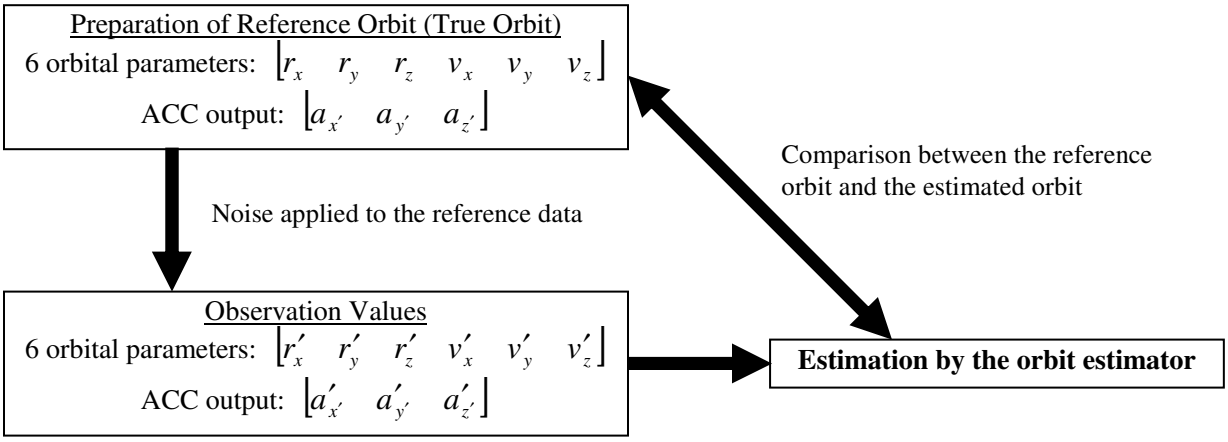

Figure 5-1-1: Diagram of Simulation Configuration

As Figure 5-1-1 shows the reference orbit called "true orbit" is prepared at first. In real situation nobody knows the "true" orbit. The force model for the true orbit is summarised in Table 5-1-1.

The geo-potential model used in this study is WGS 84 (EGM 96). Two disturbing forces by the Sun and the Moon are included. The coefficient of the air drag changes from 0.0 to 1.99e-13 because of the atmospheric density model applied to this study. On the other hand the coefficient of the solar radiation pressure is set to constant number. Note that the orbit estimator simply assumes that those coefficients of the air drag and the solar radiation pressure are constant.

However, the real coefficients are not constant. They change depending on the solar activity whose magnitude is usually unpredictable, although the cycle of the period of the solar maximum and minimum is not unknown.

Table 5-1-1: Force Model of True Orbit

Geo-potential Model	36 x 36
3-Body Disturbing Forces	Sun & Moon
Coefficient of Air Drag	0.0 ~ 1.99e-13
Coefficient of Solar Radiation Pressure	3.53e-10

5-2 Simulation Cases

5-2-1 Case1: Influence of GPS Positioning Accuracy

Here we can see the influence of the GPS positioning accuracy to the orbit determination error. Table 5-2-1-1 shows the relationship between the noise configurations of GPS positioning and the orbit determination errors when the orbit is determined only by the GPS measurement data. The initial coefficient of the air drag is set to 0.0 and the coefficient of the solar radiation pressure is 7.06e-10 which is twice larger than the true value.

Table 5-2-1-1: GPS Positioning Accuracy and Orbit Determination Error

Case Number		Case 1-1	Case 1-2	Case 1-3
GPS positioning random error [m]	Along	0.02	0.20	2.00
	Cross	0.02	0.20	2.00
	Radial	0.04	0.40	4.00
Orbit Determination Error [m]		8.19	9.29	16.32

The result tells us that the orbit determination error will be more than 8 m even if we use a very accurate GPS receiver whose positioning accuracy is only 2.0 cm in the along and cross track, and 4.0 cm in the radial. When we use an ordinal GPS receiver such as 2.0 m positioning accuracy the determination error increases up to about 16 m.

5-2-2 Case2: Influence of Initial Coefficients

To figure out the influence of the initial coefficients to the orbit determination accuracy, three cases with different initial coefficient are simulated. Note that the coefficient of the air drag is set to 0.0 because the air drag is basically zero except the small part of the orbit near perigee. Table 5-2-2-1 summarises the result.

Table 5-2-2-1: Initial Coefficients and Orbit Determination Error

Case Number		Case 2-1	Case 2-2	Case 2-3
Initial Coefficients	Air Drag	0.0	0.0	0.0
	Solar Radiation Pressure	7.06e-10*	1.77e-9**	3.53e-9***
Orbit Determination Error [m]		8.19	31.36	75.60

* True value x 2, ** True value x 5, *** True value x 10

When we see the result we can easily find that the influence of the initial coefficient are very large. If we use the value which is ten times larger than the true one the determination error becomes 75.6 m. Perhaps the reader of this paper may think that this difference is "too large". However the real coefficients of the air drag and the solar radiation pressure are very small so the tens or hundreds times variation is not unusual.

5-3 Simulation Result

5-3-1 Contribution of ACC

To improve the orbit determination accuracy, an on-board ACC is used. When the ACC is available we can get the information of the non-conservative force vectors i.e. the air drag and the solar radiation pressure. The information from the ACC allow us to estimate more suitable coefficients, which update the force model used in the orbit estimator and improve the determination accuracy. Figure 5-3-1-1 shows the orbit determination error at apogee by the estimation with using the on-board ACC.

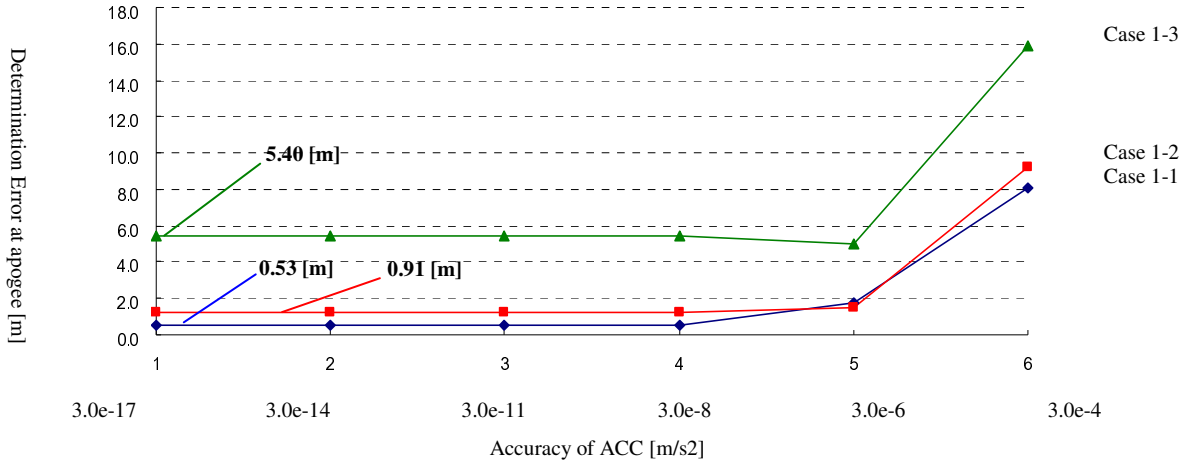

(a) Case 1

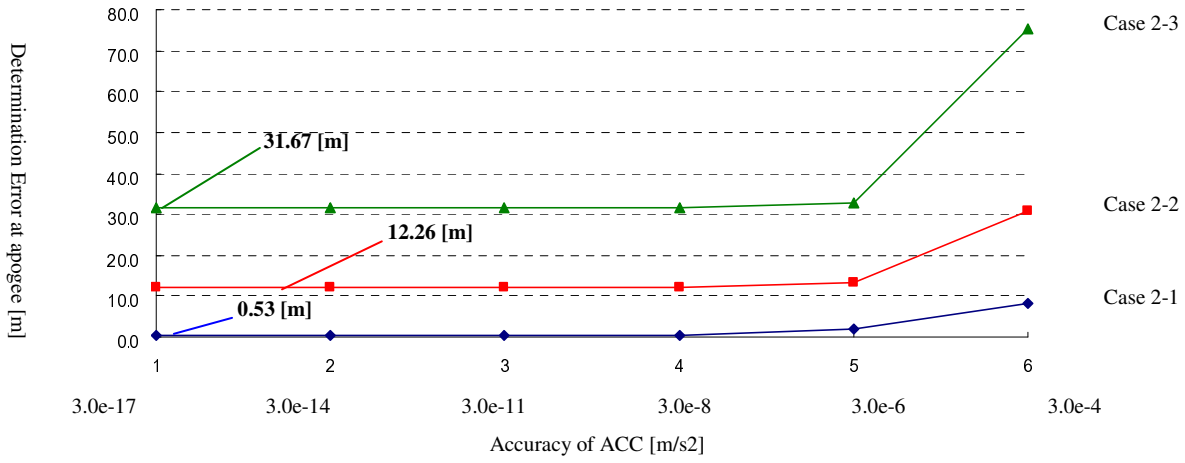

(b) Case 2

Figure 5-3-1-1: Result of Orbit Determination with ACC

The horizontal axis shows the accuracy of the on-board ACC and the vertical axis shows the orbit determination error at apogee. Figure (a) is the result of Case 1, which shows the errors with three different GPS positioning accuracies and the contribution of the on-board ACC to the orbit determination precision. Figure (b) is the result of Case 2 showing the errors with three different initial coefficient set.

At first let's see the result of Figure (a). As you can see the determination accuracy significantly improves by the use of the ACC. When we use the hybrid method with an super accurate GPS receiver with 2.0 cm

positioning accuracy and a ultra accurate ACC with 3.0e-17 m/s2, then we can determine the orbit in an accuracy of 53.0 cm at apogee. Even in the worst case whose determination error is about 16 m when it is determined only by GPS, the error decreases down to 5.4 m.

On the other hand, Figure (b) shows the necessity of the accuracy of the initial coefficient. As it was said in the previous section the influence of the initial coefficient to the orbit determination accuracy is very large. Even if a very accurate ACC is used for the estimation the determination error still remains more than 30 m when the initial value which is ten times larger than the true value is used. In other words, this result tells us that we have to determine the initial coefficient as precisely as possible if we need to fit the orbit accurately.

5-3-2 Estimation of the Coefficient of Air Drag

As you already know, the orbit estimator of this study estimates the two coefficients of the air drag and the solar radiation pressure.

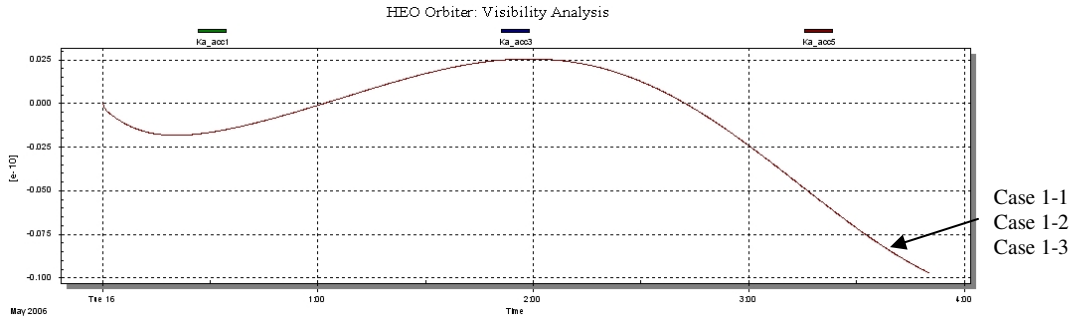

(a) Case 1

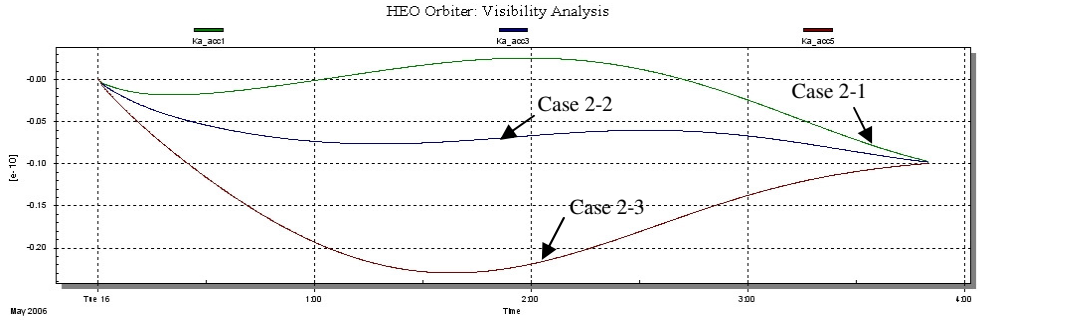

(b) Case 2

Figure 5-3-2-1: Result of Estimation of Air Drag Coefficient

Here the estimation result of the air drag's coefficient is shown. Figures 5-3-2-1 show the results of the estimation with four different ACCs. Similarly to the previous section Figure (a) corresponds to Case 1 and Figure (b) is the result of Case 2. The horizontal axis shows the time period starting on 00:00:00.0, 16th, May, 2006. The estimation time period is roughly 4 hours which corresponds to the half of the period of ASTRO-G's orbit. The vertical axis shows the value of the estimated coefficient.

When we scrutinise the results shown in Figure (a) we find that the estimated value is negative number i.e. "-9.72e-12" at the end of the estimation time period. Frankly speaking this result is odd because the coefficient should always be positive value.

However, in this study a very simple atmospheric density model is applied. According to the density model the air density has some value when the user satellite's altitude is below 1,750 km, but in the most of the part of the orbit this value is zero. In contrast, the orbit estimator simply assumes the coefficient is a constant value. Hence the estimator has to make the value negative to cancel the effect of the air drag applied to the user satellite near perigee. This is the why.

Figure (b) also shows a similar result. The three lines appearing in the graph correspond to Case 2-1, Case 2-2 and Case 2-3 respectively. According to the result all of the three values converge to the same value as Figure (a) i.e. "-9.72e-12". On the other hand, the shape of the three lines are different each other while those in Figure (a) are perfectly same. This is because of the initial coefficient of the solar radiation pressure. The force sensed by the on-board ACC consists of the air drag and the solar radiation pressure, so the different coefficient of the solar radiation pressure affects to that of the air drag.

5-3-3 Estimation of the Coefficient of Solar Radiation Pressure

Here we see the estimation result of the solar radiation pressure's coefficient. Figures 5-3-3-1 show the result.

Figure (a) shows us the good estimation result of the coefficient. The value converges to "3.32e-10" while the true one is "3.53e-10". The shapes of the lines of those three different cases are completely same, which means the influence of the GPS positioning accuracy to the estimation of the coefficients are very small.

Conversely, Figure (b) shows different characteristic. In Figure (b) the estimated values of the coefficient in those three cases are different each other. Obviously this is because of the initial coefficient set. The solar radiation pressure's coefficients of Case 2-1, Case 2-2 and Case 2-3 converge to "3.3e-10", "4.5e-10" and "6.6e-10" respectively, while the true one is "3.53e-10". The difference of those values are very small, but those small variations of the estimated coefficients cause the large orbit determination error as you saw in the previous section.

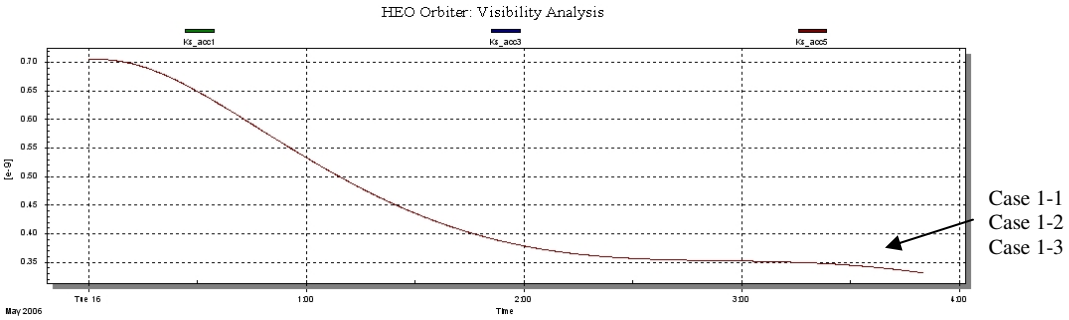

(a) Case 1

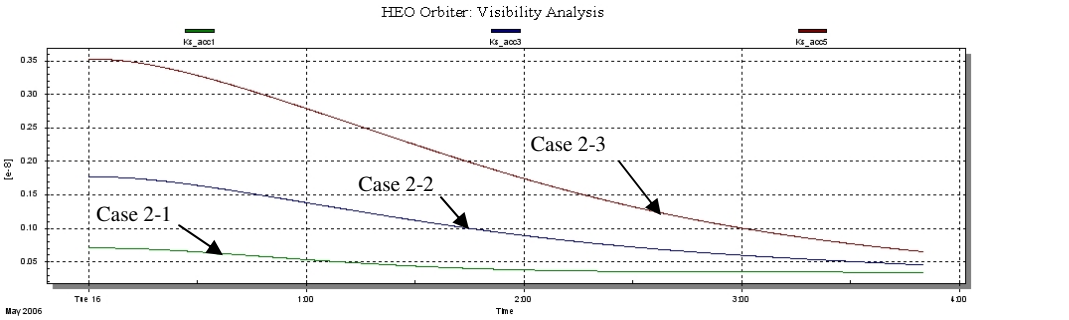

(b) Case 2

Figure 5-3-3-1: Result of Estimation of Solar Radiation Pressure Coefficient

5-4 Influence by ACC's bias

In this study, the following ACC bias model is applied as a test.

$$Bias = b + \dot{b}(t_{ref} - t) + \ddot{b}(t_{ref} - t)^2 \tag{5-4-1}$$

At this present time the research for the ACC's bias is not sufficient. However, by using the brief model described in the equation (5-4-1) the influence by the bias was tried to figure out.

Table 5-4-1: Values of ACC bias

Bias	Values
b	2.0e-11
$\dot{b}$	2.0e-14
$\ddot{b}$	2.0e-17

In this study the accuracy of GPS is same as case1-1 in Table 5-2-1-1. The random noise of ACC is 3.0e-11. The initial coefficients of the air drag and the solar radiation pressure of the estimator are twice larger than the true value. In this case the peak range error became about **3.63m** while that of the same case without ACC bias is about **0.53m**. To reduce this error the ACC bias should also be estimated by the estimator.

6. Conclusion

This study revealed the feasibility of the hybrid orbit determination method by GPS and ACC. If only GPS measurement data is used for the determination at least 8 m error will emerge at apogee even if a super accurate GPS receiver is used. However the ACC allows us to estimate the coefficients of the non-conservative forces i.e. the air drag and the solar radiation pressure applied to the user satellite, which reduces the determination error down to only 53 cm. This study also tells us that the more accurate ACC makes the determination accuracy better, but the contribution of the ACCs which are more accurate than "3.0e-8 [m/s2]" saturates.

The influence of GPS positioning accuracy to the orbit determination error is not small. A few meters positioning error at perigee will produce about 16 m error at apogee. This accuracy should be taken into account through the use of dual frequencies, a more detailed Kalman filter capable of modelling the clock bias model of the GPS receiver when we need to determine the orbit precisely. The use of GPS weak signals from the side lobe of the transmission antenna may also be useful to achieve better result.

The biggest factor which affects to the determination accuracy is the initial coefficients set of the air drag and the solar radiation pressure. Generally speaking, these values are so small that the ten or hundred times variations of those values are common. However this study revealed the ten times difference will cause more than 75 m error at apogee. Hence it is vitally important to set those initial coefficients as precisely as possible if a very accurate orbit determination accuracy is required.

As future works, the problem of an ACC's bias still remains. In real situation the output data from an on-board ACC contains some bias which changes over time. This problem should be discussed when this method is applied to the application of real spacecrafts. To solve this problem it is intended to estimate the ACC's bias as well as other state parameters. The bias model should be considered for the modification.

The calibration of the on-board ACC is also important problem. This also should be taken into account to make this algorithm more practical.

References

1. "Fundamentals of astrodynamics and applications, 2nd Edition" David A. Vallado, Space Technology Library

2. "Space Mission Analysis and Design, 3rd Edition" James R. Wertz and Wiley J. Larson, Space Technology Library

3. "Advanced Engineering Mathematics, 9th Edition" Erwin Kreyszig, John Wiley & Sons, INC

4. "Understanding GPS: Principles and Applications, 2nd Edition" Elliott D. Kaplan and Christopher Hegarty, Artech House

5. "Fundamentals of Global Positioning System Receiver A Software Approach, 2nd Edition" James Bao-Yen Tsui, Wiley-Interscience

6. "Annual Report 1992 GPS Navigation FjSAT project" Yoshikazu Hashida, Fujitsu & Surrey Satellite Technology Ltd internal document

7. "Mathematical Specification of Experiment Orbit Determination of MEO by GPS REVISION 1" Yoshi Hashida, Surrey Satellite Technology Limited Internal Technical Note

8. "Mathematical Specification of Experiment Orbit Determination of GEO by GPS REVISION 1" Yoshi Hashida, Surrey Satellite Technology Limited Internal Technical Note

9. "ADCS for Future UoSat Standard Platform REVISION 2, August 24, 2004" Yoshi Hashida, Surrey Satellite Technology Limited Internal Technical Note

10. "Electrostatic Accelermeters For The Equivalent Principle Test in Space" P Touboul, M Rodrigues, E Willemenot and A Bernard, Office National d'Etudes et de Recherches Aerospatiales, France

11. "Results from the GPS Flight Experiment on the High Earth Orbit AMSAT OSCAR-40 Spacecraft" Michael C. Moreau (1), Edward P. Davis (1), J. Russell Carpenter : (1), David Kelbel (2), George W. Davis (3), Penina Axelrad (4)(1) NASA Goddard Space Flight Center, (2) Computer Sciences Corporation, (3) Emergent Space Technologies, (4) University of Colorado at Boulder

12. "Possibility of Laser Ranging Support For The Next-Generation Space VLBI Mission, ASTRO-G" Toshimichi Otsubo (1), Toshihiro Kubo-oka (1), Hirobumi Saito (2), Hisashi Hirabayashi (2), Takaji Kato (2), Makoto Yoshikawa (2), Yasuhiro Murata (2), Yoshiharu Asaki (2) and Shin-ichi Nakamura (3) : (1) Kashima Space Research Center, National Institute of Information and Communications Technology, (2) Institute of Space and Astronautical Science, Japan Aerospace Exploration Agency, (3) Consolidated Space Tracking and Data Acquisition Department, Japan Aerospace Exploration Agency